Imaging Characteristics of Normal Liver and Liver Tumors

2

Ali A. Haydar, MD, MRCP, FRCR, Layla Antoine Nasr, MD and Hero K. Hussain, MD, FRCR, FACR

Abbreviations

US	Ultrasound
CT	Computed tomography
MRI	Magnetic resonance imaging
FDG-PET	Fluorodeoxyglucose, positron emission tomography
MDCT	Multidetector computed tomography
MRCP	Magnetic resonance cholangiopancreatography
ERCP	Endoscopic retrograde cholangiopancreatography
GRE	Gradient recalled echo
DWI	Diffusion-weighted imaging
ADC	Apparent diffusion coefficient
HCC	Hepatocellular carcinoma
IVC	Inferior vena cava
RES	Reticuloendothelial system
TIPS	Transjugular intrahepatic portosystemic shunt
GI	Gastrointestinal
AASLD	American Association for the Study of Liver Disease
LI-RADS	Liver imaging reporting and data system

A.A. Haydar (✉)
Department of Radiology, American University of Beirut Medical Centre, Bliss Street, Beirut 1107 2020, Lebanon
e-mail: ah24@aub.edu.lb

L.A. Nasr
Department of Diagnostic Radiology, American University of Beirut Medical Center, 2139 Orchard Lakes Pl E, Apt 31, Toledo, OH 43615, USA
e-mail: lan03@mail.aub.edu

H.K. Hussain
Department of Radiology, University of Michigan Health System, Ann Arbor, MI, USA

2.1 Anatomy

2.1.1 Gross Anatomy and Landmarks

The liver lies in the upper abdomen and extends from the epigastrium medially to fill the right hypochondrium. Its superior surface is dome-shaped and follows the contour of the diaphragm lying approximately at the level of the fifth rib. Its anterior surface extends down to the right costal margin.

J. Meyer and T.E. Schefter (eds.), *Radiation Therapy for Liver Tumors*,
DOI 10.1007/978-3-319-54531-8_2

The major landmark of the superior surface of the liver is the sagittal groove, which is the notch for ligamentum teres (formerly the umbilical vein), and lies at the free edge of the falciform ligament. The major landmark of the inferior or visceral surface is the porta hepatis, which is a central depression that accommodates the portal vein, hepatic artery and common bile duct [1, 2].

2.1.2 Liver Size

The weight of a normal liver is approximately 2% that of total adult body weight [3]. CT Liver volumetric measurements are useful to assess the functional residue of the liver prior to resection and the volume of the liver in transplant donors. Using commercially available software, measurements may be done manually, or by semi-automated or automated programs, the latter requiring significantly less time. Individual lobar and segmental volumes can also be measured. Enhanced CT in the venous phase is the preferred phase to measure and segment the liver due to better delineation of blood vessels [4].

2.1.3 Segments and Vascular Supply

The liver receives approximately 75% of its blood supply from the portal vein and 25% from the hepatic artery, while blood drains via three main hepatic veins into the IVC. The pressure difference between measurements in the wedged (occluded) hepatic vein and the IVC (also known as the corrected sinusoidal pressure) is normally between 4 and 8 mmHg. This pressure measurement can be used to evaluate liver disease, namely cirrhosis [5].

The liver is divided into eight functional segments according to the Couinaud classification. Each of these segments receives a branch of the portal vein, is bounded by a hepatic vein [6], and has its separate hepatic arterial branch and bile duct [3]. The major landmarks used to divide the liver into its functional segments are the portal and the hepatic veins. The main portal vein divides the liver axially into two virtual superior (segments VII, VIII, IVa, and II) and inferior parts (VI, V, IVb, and III). The middle hepatic vein divides the liver into left and right lobes. The left hepatic vein runs vertically and separates the left lateral and left medial segments of the liver. The plane of the left portal vein divides the lateral segment into superior segment II and inferior segment III, and the left medial segment into superior segment IVa and inferior segment IVb. The right hepatic vein divides the right lobe into anterior segments V/VIII and posterior segments VI/VII. The plane of the right portal vein divides the right lobe into superior segments VII and VIII, and inferior segments V and VI. Segment I (caudate lobe) receives portal supply from both lobes and drains directly to the IVC [2, 7].

2.2 Liver Imaging Techniques and Imaging of the Normal Liver

2.2.1 Plain Radiography

The complex shape of the liver and limited soft tissue contrast of plain radiographs makes reliable identification of the liver boundaries difficult. Even though significant findings such as gross hepatomegaly, hepatic calcification, and pneumobilia may be detected on plain films [8], further evaluation with other modalities would most likely be needed.

2.2.2 Ultrasound

Ultrasound (US) of the liver is performed using a phased array transducer operating between 3 and 5 MHz Doppler capabilities [9]. The normal echotexture of the liver parenchyma is homogeneous and slightly more reflective than the adjacent renal cortex. Scanning the liver in all directions in deep inspiration is essential to cover its entire span and detect inconspicuous lesions. In case a lesion is found, intravenous injection of a microbubble intravascular contrast agent can improve its characterization by observing the arterial and portal phases of enhancement.

The gallbladder, intra- and extrahepatic bile ducts are also routinely assessed by US for dilatation and presence of stones. In addition, Doppler interrogation of the liver vasculature is routinely performed to visualize the portal flow phasicity and measure its velocity. Portal vein branches may be identified by their radiating pattern from the hilum and the increased reflectivity of their walls. In contrast, hepatic veins radiate from the inferior vena cava and their walls are not distinguishable from the adjacent parenchyma. On Doppler examination, the normal hepatic vein trace reflects the transmitted right-heart pressure changes with reversal of flow during the cardiac cycle. Ultrasound is also used to assess the patency and flow velocity of the hepatic artery and its branches [10].

2.2.3 Computed Tomography

The liver appears homogeneous on non-contrast computed tomography (CT) with attenuation values of 55–65 HU, approximately 8 HU greater than the spleen. The vascular structures of the liver, the common bile, common hepatic, and right and left hepatic ducts are easily identified on contrast-enhanced CT, while the peripheral intrahepatic ducts are not. Multiphasic, multidetector CT (MDCT) scan is commonly used to assess the liver and characterize liver lesions. This technique typically includes an arterial-dominant phase at 10–30 s post contrast injection, a portal or venous phase at 60–90 s post contrast injection, and a delayed phase at 5–10 min post contrast injection. An unenhanced scan is optional and not routinely performed at all centers. The minimum requirement is an arterial phase and a portal/venous phase; however, the delayed phase is of great value in the characterization some benign and malignant lesions (e.g., hemangioma and cholangiocarcinoma) [2]. Optimizing the protocols and timing of these phases are important to maximize lesion-to-liver contrast. For this purpose, a method known as automatic bolus tracking is used to time the arterial phase; scanning is triggered when contrast is, for example, detected in the celiac axis or hepatic artery. This technique gives more consistent results and accounts for the variation in cardiac output and intravascular volume [11].

Cone beam CT is basically a CT scan performed with catheter injection into the hepatic artery in the angiography suite to detect subtle liver lesions or to guide treatment used mainly in oncology liver directed therapies such as transarterial chemoembolization [12].

2.2.4 Magnetic Resonance Imaging

Magnetic resonance imaging (MRI) has several advantages over CT and US for imaging the liver. First, it lacks ionizing radiation. Second, it has excellent soft tissue contrast and is therefore preferred for lesion detection and characterization. Third, it clearly delineates the biliary system and the hepatic vascular anatomy and patency. MRI has a wider range of tissue contrast and contrast media compared to other imaging techniques due to a combination of field strength, pulse sequences, interdependent sequence parameters, and the availability of liver-specific contrast agents. All of these factors serve to strengthen image quality [13, 14].

Multichannel phased array coils are routinely used for imaging the liver. When performing MR sequences, there is always a trade-off between image resolution and scan time. Shortening scan time can compromise intrinsic contrast and spatial resolution and limit the usefulness of MRI for lesion detection and characterization. Comprehensive liver MR imaging includes breath-hold T1-weighted (T1W) in-phase and out-of-phase gradient-recalled echo (GRE) imaging sequences for lipid detection and lesion characterization, and breath-hold T2-weighted (T2W) imaging using a turbo spin-echo sequence, usually single shot. Higher quality T2W images are acquired with respiratory-triggered multishot sequences. Also, quantitative diffusion-weighted imaging (DWI) and apparent diffusion coefficient (ADC) calculations are increasingly being studied for their role in lesion detection and characterization [15]. Multiphasic contrast-enhanced

T1W GRE imaging is routinely performed in all MRI studies of the liver.

The intensity of normal liver parenchyma is the same as, or slightly higher than, that of adjacent muscle on T1- and T2-weighted imaging. The liver–spleen differences may serve as a simple guide to the efficacy of intrinsic T1 and T2 weighting. Generally, the spleen should be lower signal (darker) than liver on T1W images and higher signal (brighter) on T2W imaging. The appearance of vessels varies widely on MRI depending on pulse sequence and on the use of artifact suppression techniques or contrast media. In particular, intravascular signal on conventional spin-echo sequences may occur normally and should not be interpreted as thrombus without confirming on other sequences. Finally, the bile ducts are best imaged using a dedicated magnetic resonance cholangiopancreatography (MRCP) technique with fluid-sensitive, heavily T2-weighted imaging [16].

For contrast-enhanced images, Gadolinium-based non-specific extracellular contrast agents are injected intravenously and provide enhancement on T1W images in a similar fashion to iodinated contrast media at CT examination. For example, breath-hold T1W sequences allow the acquisition of multiphasic (arterial, portal/venous, delayed) images. The enhancement characteristics of many focal lesions are similar to CT. Several liver-specific contrast agents are increasingly being used but have not yet made it to the guidelines for liver lesion characterization. Hepatocyte-specific gadolinium-based agents accumulate in hepatocyte and are excreted in bile via specific receptors on the hepatocytes. They result in enhancement of the normal liver parenchyma and biliary system on T1W imaging and serve as an indicator of the presence of and the function of hepatocytes. Liver-specific agents that are taken up by Kupffer cells, which represent the reticuloendothelial system (RES) of the liver, have also been developed [17].

2.2.5 Nuclear Imaging

Radionuclide imaging of the liver is performed using ^{99m}Technetium-sulfur colloid or albumin colloid, which are taken up by the reticuloendothelial system. Liver scintigraphy is seldom used as a primary diagnostic investigation but can help characterize focal lesions when MRI and CT are not available [18]. PET and PET/CT are not frequently used to identify malignant liver lesions. Their main role in imaging primary liver neoplasms, particularly hepatocellular carcinoma, is for the assessment of extrahepatic metastasis. For cholangiocarcinoma, PET-CT offers no added benefit compared to CT and MRI/MRCP in detecting the primary tumor. In fact, it is inferior to MRI especially in detecting primaries of the extrahepatic biliary duct. The only instance where nuclear imaging would be more reliable is in detecting distant metastatic disease from cholangiocarcinoma [19].

2.2.6 Invasive Liver Imaging

The hepatic arteries are best visualized by selective catheterization.

The hepatic veins can be routinely seen on digital subtraction angiography. However, for direct visualization, they are catheterized retrogradely, using a femoral or jugular approach and venography is obtained with the catheter free in the veins. Wedged hepatic venous pressure measurement is performed following impaction of an end-hole catheter in a small branch of a hepatic vein. The catheter position is confirmed by the injection of contrast medium, which produces parenchymal staining [20].

The portal system is not normally visualized on a selective hepatic arteriogram unless there has been flow reversal or an arterioportal shunt. Therefore, it is accessed directly by a catheter or needle inserted into a portal vessel percutaneously under ultrasound guidance, or indirectly by selective injections into the celiac, splenic, superior mesenteric, or inferior mesenteric arteries. Direct methods (including percutaneous splenic, transhepatic and transjugular approaches) are now used only when therapeutic procedures [e.g., Transjugular Intrahepatic Portosystemic Shunt (TIPS)] or sampling techniques (e.g., direct portal venous pressure measurement) are needed.

Cholangiography can be performed retrogradely via an endoscopic approach [Endoscopic Retrograde Cholangiopancreatography (ERCP)] or percutaneously by placing a needle or catheter through the liver parenchyma into the bile ducts. Diagnostic MRCP has largely replaced the invasive diagnostic methods for imaging the biliary system. These invasive methods are now performed as part of therapeutic interventions to drain an obstructed biliary tree [21].

2.3 Imaging of Liver Cirrhosis (Table 2.1)

2.3.1 General Imaging Features of Cirrhosis

Regardless of etiology, gross morphologic changes of advanced cirrhosis are well recognized by any cross-sectional technique such as US, CT, or MRI. These encompass hepatomegaly in the early stages, shrinkage of the right lobe with enlargement of the lateral segment of the left lobe and caudate lobe, and nodularity of the surface contour [22].

On US examination, the liver contour may appear nodular with coarse echotexture. Flow dynamics of the hepatic vasculature may also be altered. These alterations are evaluated with Doppler sonography. In the hepatic artery, the resistive index is either increased due to compression by cirrhotic liver parenchyma, or decreased due to spontaneous arteriovenous shunt formation. The latter is more specific for cirrhosis [10]. Changes also occur in the portal flow in the setting of portal hypertension (see the next section). The portal flow slows down (velocity less than 15 cm/sec), becomes stagnant, or is reversed; this reversal is termed "hepatofugal flow" [23]. Finally, the hepatic venous circulation loses its phasicity and ceases to reflect right atrial pressure changes [10].

On CT imaging (Fig. 2.1), the cirrhotic liver appears enlarged in the early stages and shrunken in severe cirrhosis. As cirrhosis advances, the liver margins appear nodular, and the organ becomes diffusely heterogeneous because of the fibrotic changes in its parenchyma [24]. Regenerative nodules are difficult to see on non-contrast CT, unless they contain iron (siderotic nodules) which makes them hyperdense relative to the

Table 2.1 Imaging findings of liver cirrhosis

Ultrasound	CT	MRI	Angiography
– Hepatomegaly (early) – Irregular contour – Right lobe and medial left lobe atrophy; lateral left lobe and caudate lobe enlargement – Coarsened echotexture – Arteriovenous shunts – Hepatic arteries: increased or decreased resistive index; dilation and tortuosity – Portal veins: slow flow, stagnancy, or hepatofugal flow – Hepatic veins: loss of phasicity – Splenomegaly – Ascites – Portovenous collaterals	– Hepatomegaly (early) – Irregular contour – Right lobe and medial left lobe atrophy; lateral left lobe and caudate lobe enlargement – RN/SN/fibrosis – Arteriovenous shunts – Splenomegaly – Ascites	– Hepatomegaly (early) – Irregular contour – Right lobe and medial left lobe atrophy; lateral left lobe and caudate lobe enlargement – RN/SN/fibrosis – Arteriovenous shunts – Splenomegaly – Ascites	– Early: mildly stretched hepatic arteries – Advanced: tortuosity and "corkscrew" appearance of arteries with sudden loss in caliber; arteriovenous shunts – Portosystemic collaterals – Hepatofugal flow

Abbreviations: *RN* Regenerative Nodules; *SN* Siderotic Nodules

surrounding parenchyma. Enhanced CT may or may not reveal RNs since they do not typically enhance in the arterial phase [25]. Arterioportal shunts are often seen after contrast administration. They typically have a linear or wedge-shaped appearance and are subcapsular in location with no visible mass effect [26].

Findings on MRI (Fig. 2.2) are similar to those of CT. Additionally, fibrosis is of high signal on T2W imaging [24], and RNs have a non-specific appearance on T1W and T2W images, but sometimes contain lipid or iron. The iron-containing (siderotic) nodules show low signal on both T1W and T2W images [27].

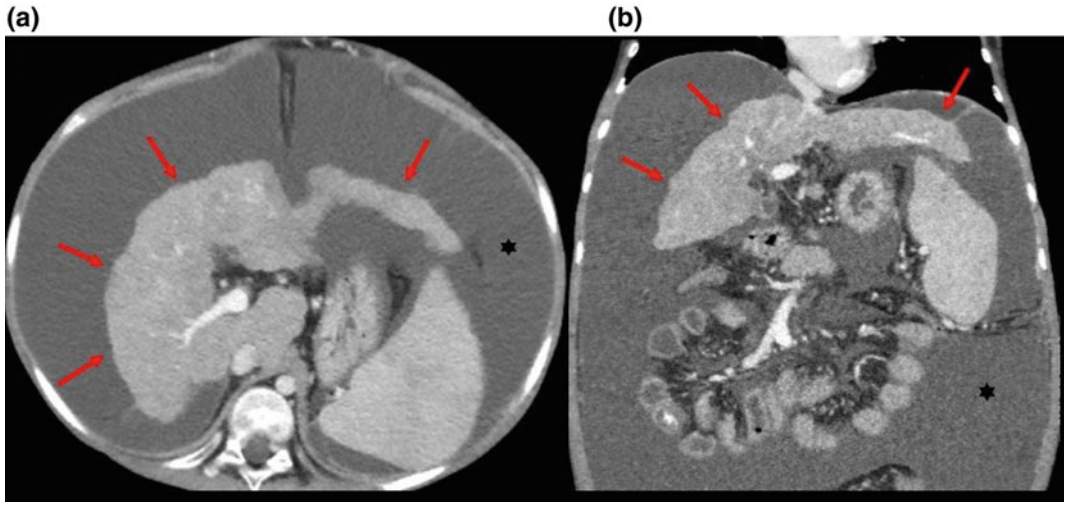

Fig. 2.1 Gross changes of liver cirrhosis seen on an axial (**a**) and coronal (**b**) images from an enhanced CT scan. The liver is shrunken with an irregular nodular contour (*arrows*) and surrounding ascitic fluid (*asterisks*)

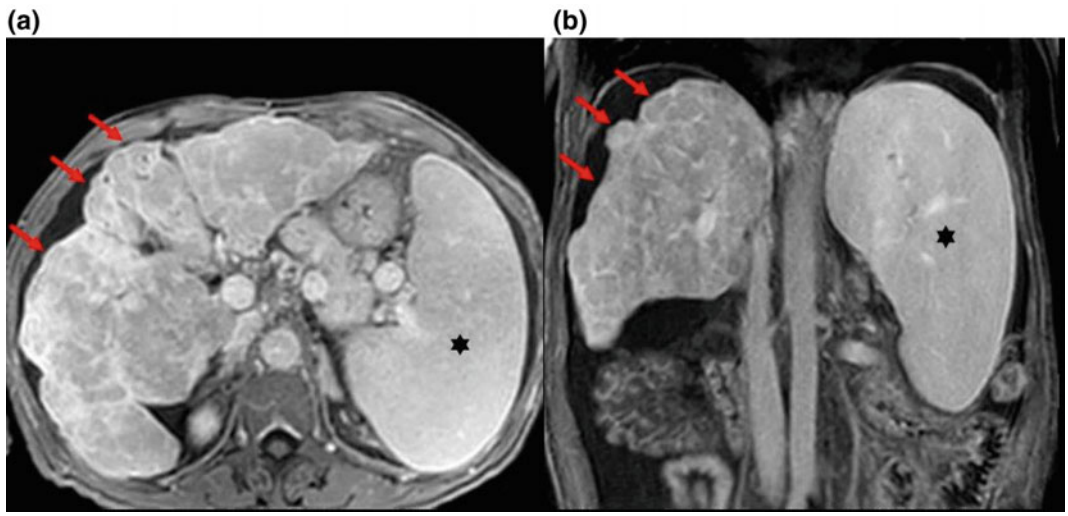

Fig. 2.2 Gross changes of liver cirrhosis seen on axial (**a**) and coronal (**b**) images from MR with gadolinium. The liver shows an irregular nodular contour (*arrows*). There is also splenomegaly secondary to portal hypertension (*asterisks*)

2.3.2 Imaging of the Effects of Portal Hypertension

The normal portal pressure measures between 4 and 11 mmHg [5]. PH is responsible for many extrahepatic manifestations of cirrhosis. It leads to splenomegaly (Fig. 2.2) with or without small nodular iron deposits within the spleen (Gamna-Gandy bodies). These deposits are related to foci of chronic hemorrhage in longstanding portal hypertension and are readily seen on MRI as foci of susceptibility artifact on GRE imaging [28]. The most specific finding of PH is the development of collateral portal venous anastomoses (varices) (Fig. 2.3). These occur in the gastroesophageal, perirectal, and retroperitoneal, with recanalization of the paraumbilical vein. When these varices develop, it is usually an indicator that the portal vein pressure exceeds 12 mm Hg. They may bleed, and the bleeding can be life-threatening. Noninvasive diagnostic imaging methods, such as color flow Doppler US, contrast-enhanced CT, and MRI can be used to identify collaterals. The major limitation of all imaging modalities is the inability to measure variceal pressure, which correlates directly with the risk of hemorrhage. Portal vein flow is altered by PH and may become stagnant. This stagnancy increases the risk of portal vein thrombosis. It is important to note that long-standing thrombosis may be associated with periportal collateral formation which re-establishes flow to the liver. This is also known as "cavernous transformation" and is a strong indication of bland thrombus in the portal vein [25]. Invasive imaging with angiography can also show the collateral flow as well as hepatofugal flow in the portal circulation [29].

2.4 Imaging of Liver Malignancies

2.4.1 Hepatocellular Carcinoma (Table 2.2)

2.4.1.1 Overview

Hepatocellular carcinoma (HCC) is the most common primary malignant neoplasm of the liver. Liver cirrhosis of any etiology is a major predisposing factor for development of HCC. HCC can be solitary, multifocal, or diffuse. The five-year survival of patients with HCC is approximately 30% [30].

On ultrasound, small HCC (<3cm) may be of increased or decreased reflectivity in relation to the adjacent parenchyma. An outer margin with a reduced reflectivity is present in some cases and thought to represent the thin fibrous capsule. Larger lesions may show internal heterogeneity, due to hemorrhagic, necrotic, or fatty components [9]. HCC may also be associated with portal vein thrombosis or intravascular tumor. Doppler examination can help distinguish tumor thrombus from bland thrombus in the portal vein:

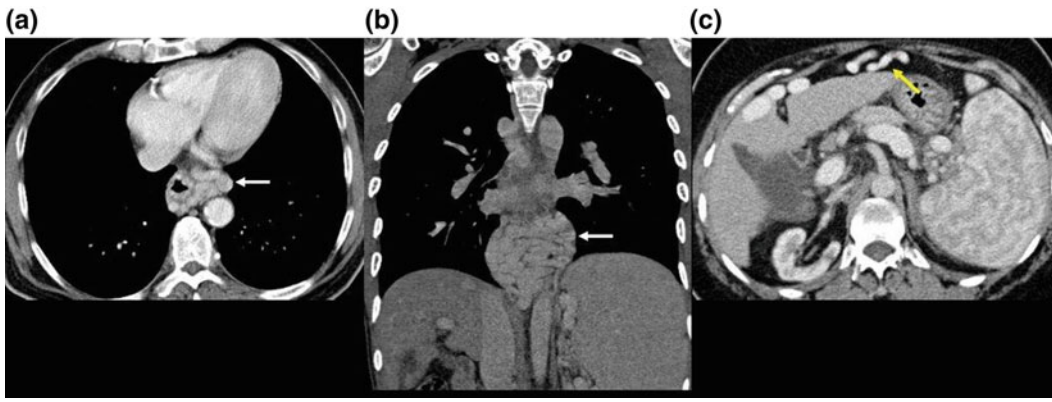

Fig. 2.3 Axial and coronal images from an enhanced CT scan (**a**, **b**) showing esophageal varices (*white arrow*). Axial image from an enhanced CT scan (**c**) showing a recanalized umbilical vein (*yellow arrow*)

Table 2.2 Imaging findings of hepatocellular carcinoma

Ultrasound	CT	MRI	Angiography
• Lesion with increased or decreased reflexivity[a] • May show thin fibrous capsule with reduced reflexivity (target sign) • Tumor thrombus in portal vein	• Non-enhanced: Ill-defined hypoattenuating; may have focal internal calcifications • Enhanced: Arterial hyperenhancement; portal venous/delayed washout and capsular appearance; tumor thrombus in portal vein	• Non-enhanced: Low T1W signal[b]; heterogeneous hyperintense T2W signal • Enhanced: Arterial hyperenhancement; portal venous/delayed washout and capsular appearance; tumor thrombus in portal vein	• Dilated feeding arteries; abundant abnormal vessels ('tumor stains')[c]; arteriovenous shunting • Translucent rim (<10% of cases) • "Threads and streaks" appearance in portal vein invasion

[a]Large lesions (≥3 cm) may show internal heterogeneity due to hemorrhagic, necrotic, or fatty components
[b]May show high T1W signal due to fat or glycogen accumulation
[c]May be hypovascular or avascular

the presence of arterial signal within the occluding material is indicative of tumor thrombus. This distinction is extremely important as tumor thrombus renders patients ineligible for liver transplantation [31]. High-velocity Doppler signals are often seen in HCC and are the result of arterioportal shunting, which is common in HCC [9].

On unenhanced CT, focal or multifocal HCC appears as ill-defined low-attenuation lesion(s). Focal areas of internal calcification have been described in up to 7.5% of lesions. Most HCCs hyperenhance relative to the liver parenchyma in the arterial phase, because they are supplied by the hepatic artery (Fig. 2.4). Some lesions enhance in a peripheral pattern around a central area of lower attenuation. Enhancement of HCC is better seen in the late arterial phase (i.e., when the portal vein becomes visible) than in the early arterial phase. The arterial phase also distinguishes tumor thrombus from bland thrombus (Fig. 2.5), because tumor thrombus enhances. In the portal venous or delayed phases, HCCs usually have lower attenuation than background liver tissue; this is known as the "washout appearance" [32]. Portal venous invasion and expansion is thought to be a specific feature of HCC. The CT features of portal venous invasion by HCC include arterioportal fistulae, periportal streaks of high attenuation, and dilatation of the main portal vein or its major branches [33].

On non-contrast MRI, HCC is typically of decreased signal on T1W images and of increased to heterogeneous signal on T2W images, depending on the size [34]. However, some lesions are of increased signal on T1W probably due to fat or glycogen accumulation. On contrast-enhanced T1W images, the enhancement patterns with gadolinium parallel those for enhanced CT examination, with most lesions hyperenhancing in the arterial phase, and becoming hypointense or washing out in the portal venous and/or delayed phases (Fig. 2.6). A delayed enhancing rim (capsule or pseudocapsule) is often seen around HCCs. Atypical regenerative and dysplastic nodules can mimic the pattern of HCC enhancement in the arterial phase and prompt uncertainty in the diagnosis.

Radionuclide imaging, including FDG-PET, is relatively non-specific for HCC and is not recommended for detecting or characterizing lesions but useful for the detection of metastatic HCC outside the liver.

Angiography shows dilated feeding arteries to the HCC, abundant abnormal vessels ("tumor stains") (Fig. 2.7), and arteriovenous shunting. Some HCC may have a surrounding capsule, and some may appear hypo- or avascular portal vein invasion produces a "threads and streaks" appearance highly suggestive of but not specific for HCC (Fig. 2.5). Angiography is used infrequently for the diagnosis of HCC because of its

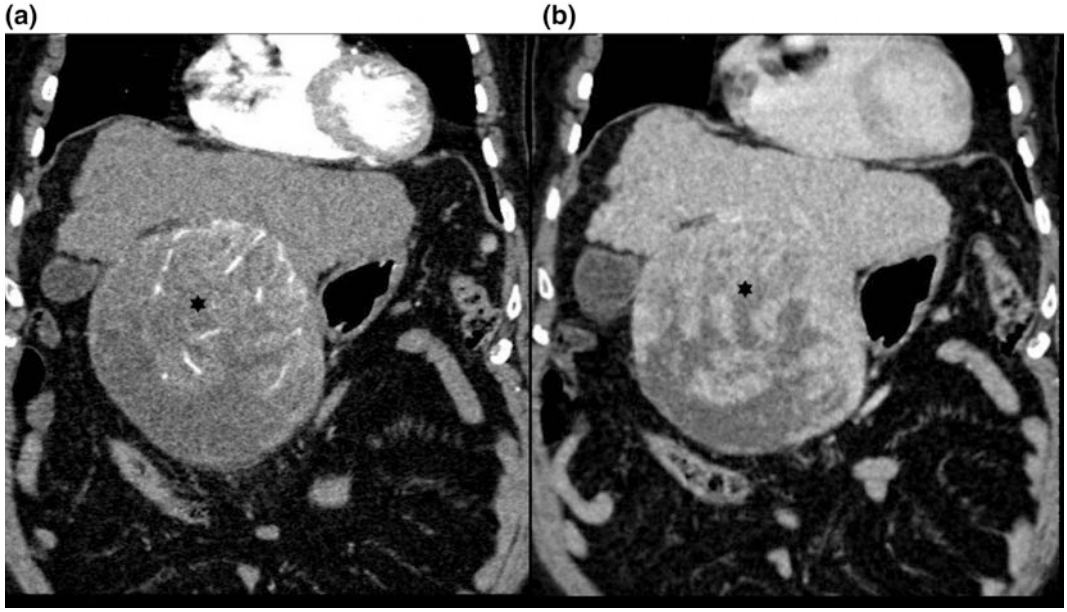

Fig. 2.4 Coronal images from a triphasic CT scan showing a large hepatocellular carcinoma (*asterisks*) with heterogeneous hyperenhancement in the arterial phase (**a**) and heterogeneous washout appearance in the portal venous phase (**b**)

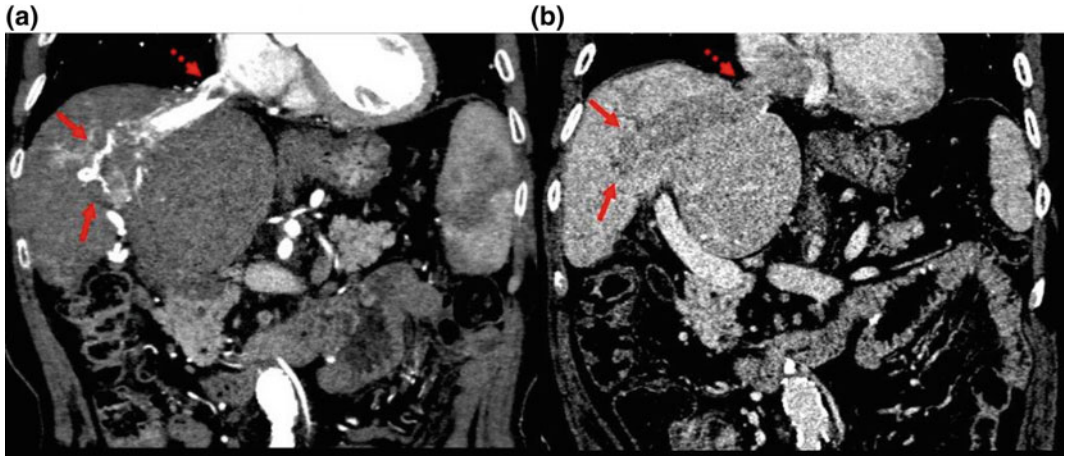

Fig. 2.5 Coronal images from a triphasic CT scan showing an HCC (*arrows*) invading the hepatic vein and extending to the right atrium (*dashed arrow*). The invading tumor exhibits a classic "threads and streaks" appearance in the arterial phase (**a**) and washout appearance in the portal phase (**b**)

invasive nature. However, it can be helpful for preoperative assessment by defining the arterial and venous anatomy and by evaluating the site and extent of portal or caval involvement when other techniques are unavailable or equivocal [35].

2.4.1.2 Detection of HCC in Cirrhotic Patients

Several guidelines and recommendations exist for this purpose. The American Association for the Study of Liver Diseases (AASLD) [36] recommends that patients with chronic hepatitis

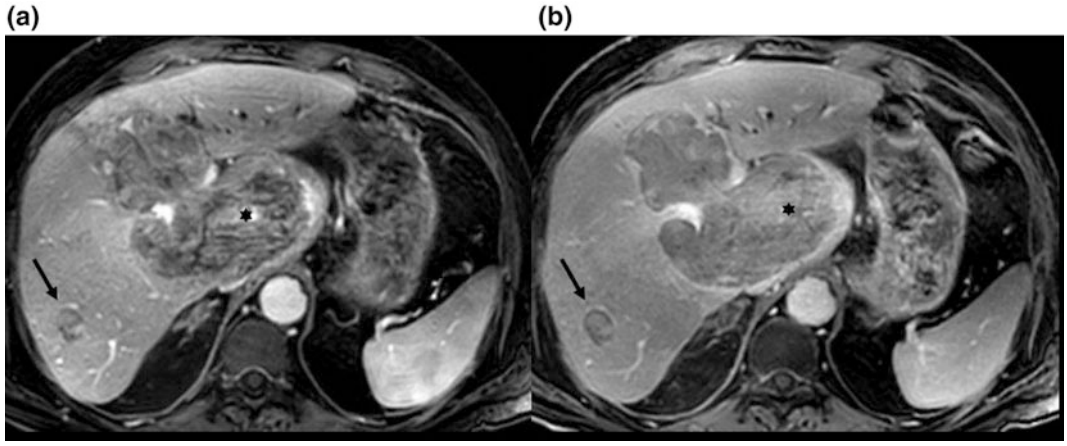

Fig. 2.6 Axial images from an MRI with gadolinium showing a large hepatocellular carcinoma (*asterisks*) and a small HCC (*arrows*) with enhancement in the arterial phase (**a**) and washout appearance in the portal venous phase (**b**)

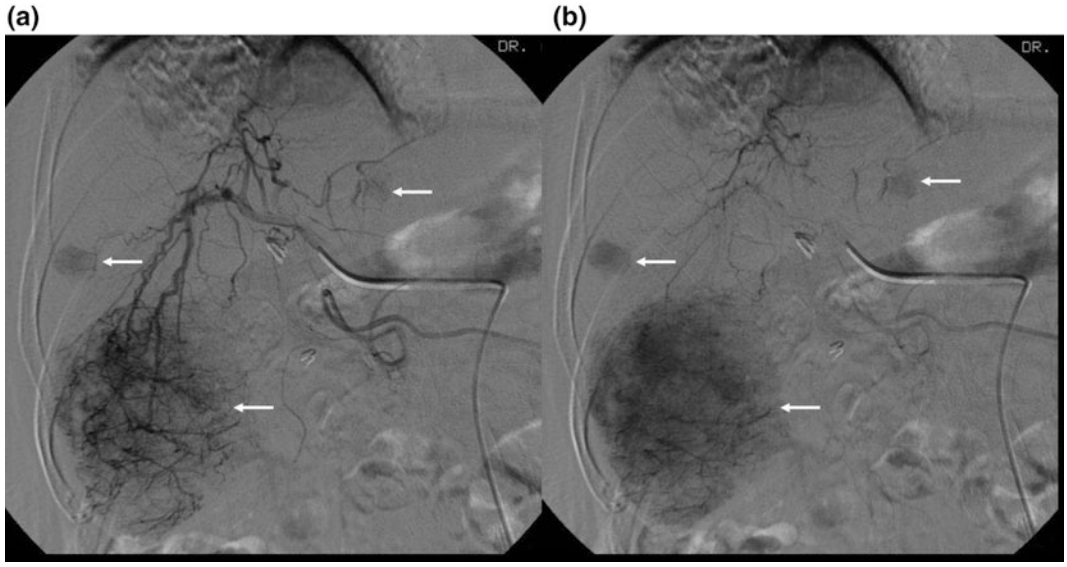

Fig. 2.7 Digital subtraction angiogram of the hepatic artery in the early (**a**) and late (**b**) arterial phases showing "tumor stains" (*arrows*) which represent multiple hepatocellular carcinomas

and/or biopsy-documented cirrhosis be screened for hepatocellular carcinoma (HCC) by ultrasound (US) at six-month intervals. CT and MRI, however, are not recommended for screening and are reserved for evaluation of certain lesions already detected on US or if an US study is equivocal or technically limited. Nodules smaller than 1 cm detected on US screening should be followed up with further US at three- to six-month intervals for two years. If no growth occurs during that interval, return to routine surveillance is recommended. However, nodules $\geq$1 cm should be investigated further with either four-phase multidetector CT or dynamic contrast-enhanced (MRI). Masses with appearances typical of HCC (e.g., hypervascular in the arterial phase with washout appearance in the portal venous or delayed phase) should be treated

as such. However, if they display an atypical behavior, they should be biopsied or imaged again with a different modalities for confirmation. If a biopsy with tumor markers proves inconclusive, they should be followed up by imaging at three- to six-month intervals until the nodule disappears, enlarges, or displays diagnostic characteristics of HCC. If they enlarge, they should be biopsied again.

The American College of Radiology (ACR) has recently supported an initiative that has helped standardize imaging in end-stage liver disease. This is known as the Liver Imaging–Reporting and Data System (LI-RADS) (see Algorithm, Fig. 2.8). The LI-RADS relies on objective criteria that are based solely on enhanced CT and/or MR imaging findings and classifies lesions in at-high-risk individuals into categories according to *probability* of malignancy. The features that are suggestive of HCC and used in the categorization are the following: (1) Mass-like appearance, (2) Arterial phase hyperenhancement (3) Washout of contrast in later phases after hyperenhancement, (4) Presence of a capsule, (5) Size of at least one cm and/or increase in one cm within one year, and (6) Tumor invasion of the portal vein. At the extreme ends of the spectrum are LR-1 and LR-5. LR-1 is a lesion that is benign with 100% certainty, such as a cyst or a hemangioma. LR-5, on the other hand, is a lesion that has a 100% chance of being HCC and satisfies at least four of the above criteria. For the other categories, LR-2 means the lesion is most probably benign with an atypical form of lesions otherwise classified in LR-1. LR-3 and LR-4, respectively, indicate an

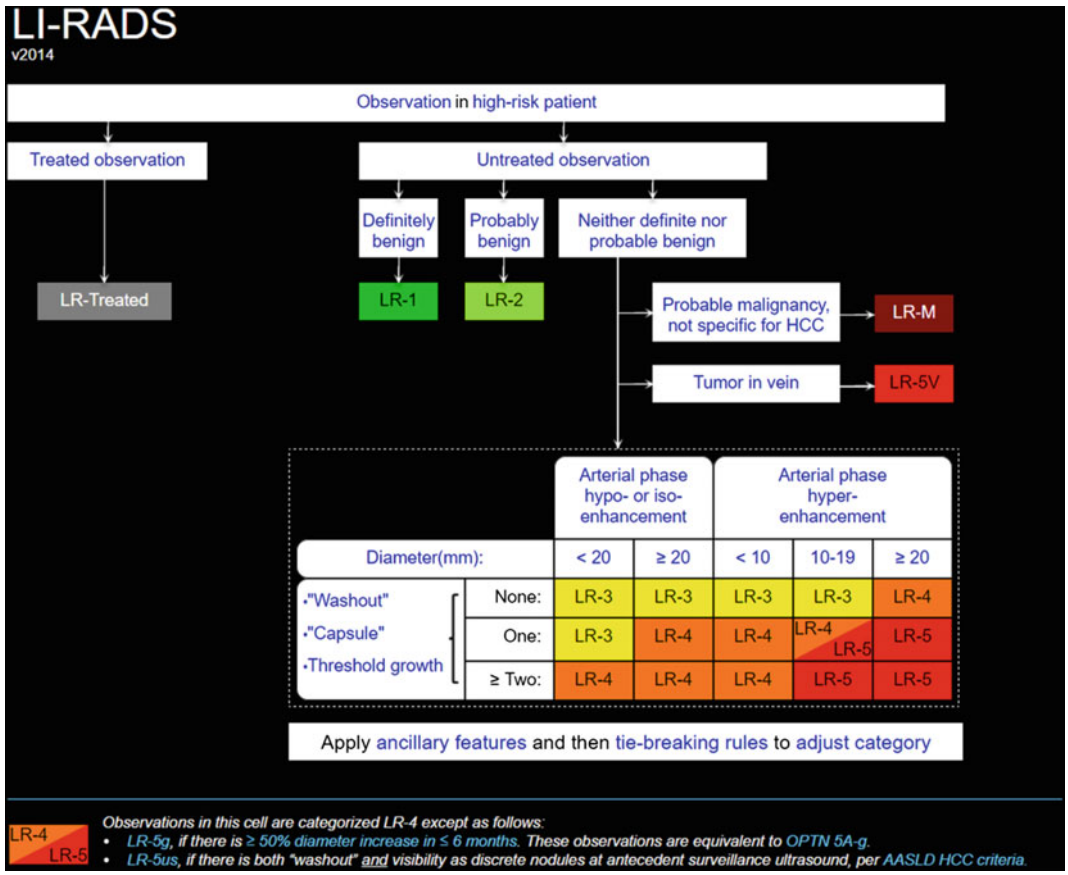

Fig. 2.8 LI-RADS algorithm [Reprinted from LI-RADS algorithm, atlas, and Lexicon, 2014. © ACR Press]

intermediate probability of HCC and a high probability of HCC; they satisfy the stated criteria to different extents. Also to note, LI-RADS includes a LR-M category which suggests the presence of a malignancy other than HCC (e.g., intrahepatic cholangiocarcinoma) [37, 38].

2.4.2 Cholangiocarcinoma

Cholangiocarcinoma is an uncommon tumor that arises from the bile duct epithelium and that tends to spread by local infiltration. Approximately 80–90% are extrahepatic (in the perihilar region (Klatskin tumors) or the distal common duct) and the rest are classified as intrahepatic or peripheral, arising within the liver and presenting as a hepatic mass [39]. The majority of tumors present with malignant hilar biliary obstruction (Fig. 2.9). Grossly, cholangiocarcinomas are classified into periductal or "infiltrating stenotic" (most common), exophytic or intraductal, or mass-forming [40]. Their appearance on imaging varies with size and pathological type [41]. Most of the infiltrating stenotic tumors are less than one–two cm in diameter, and the exophytic tumors are less than 5 cm.

On US, intrahepatic cholangiocarcinomas appear as nodules or focal bile duct wall thickening and are usually slightly hyperechoic [9]. However, in the extrahepatic types, US is much more specific in detecting bile duct dilation, an indirect imaging finding related to obstruction by the tumor [42].

On CT, the tumor nodules are usually isodense or slightly hypodense compared with liver and are more easily seen on dual-phase contrast-enhanced imaging; the infiltrating stenotic type tends to enhance in the arterial phase. The exophytic are more conspicuous on portal phase contrast-enhanced imaging, where they appear less dense than the liver. Delayed-phase imaging to 10–20 min may show late tumor enhancement. The mass-forming type shows peripheral

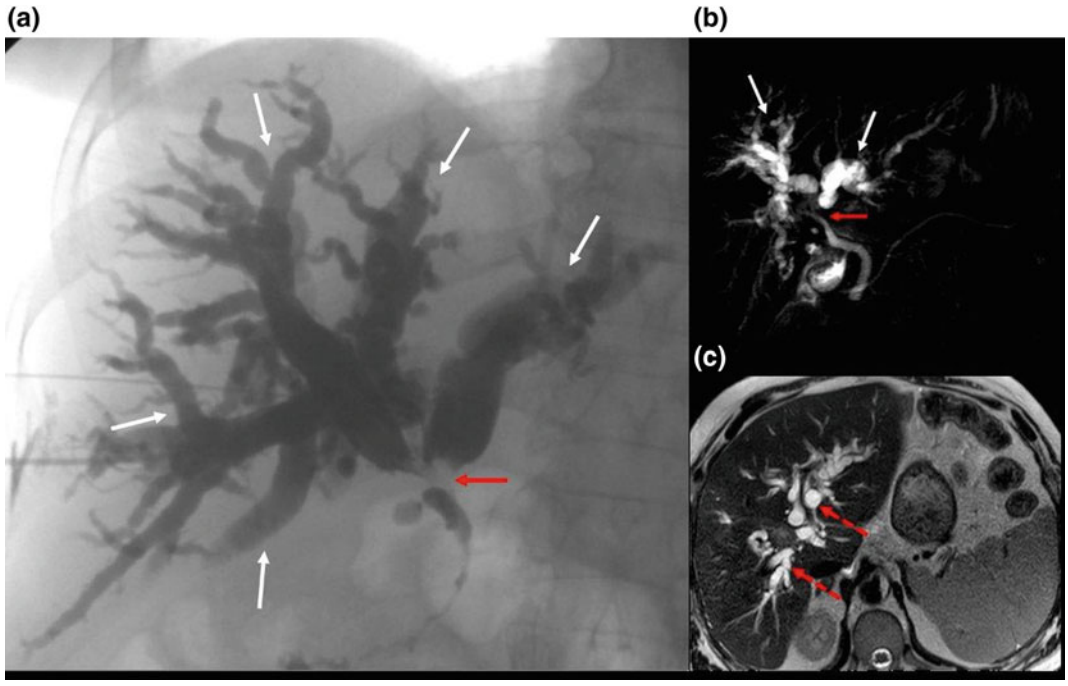

Fig. 2.9 Percutaneous Cholangiogram (**a**) and MRCP (**b**) showing a hilar obstructive lesion (*solid red arrows*) with resultant proximal biliary tree dilatation (*white arrows*). Axial T2W MR image (**c**) showing the dilated intrahepatic biliary ducts (*dashed red arrows*) with no apparent hilar lesion

enhancement on arterial phase with gradual filling in the portal and delayed phases [41].

On MRI, the tumors are hypointense on T1- and hyperintense on T2-weighted imaging and show some progressive enhancement on dynamic imaging. The most specific noninvasive modality that depicts the proximal extent of the obstruction, which critically affects treatment options, is magnetic resonance cholangiopancreatography (MRCP). In fact, it is comparable in specificity to direct cholangiography and ERCP [21].

Cholangiocarcinomas are usually hypo- or avascular, and angiography plays a minimal to no role in the diagnosis [43].

2.4.3 Metastases

The liver is one of the most common organs to which many primary malignancies from different organ systems metastasize. Hepatic metastases occur hematogenously; gastrointestinal tract tumors metastasize to the liver via the portal vein, and tumors elsewhere to the liver via the hepatic artery.

Metastases have a wide range of appearances on imaging (Fig. 2.10) but usually share the features of growth on serial imaging, multiplicity, and variation of size. Although hepatic metastases generally derive their blood supply from the hepatic artery, they can either be hypo- or hypervascular compared to the surrounding liver parenchyma. Hypervascular metastatic deposits include those from breast, kidney, thyroid, neuroendocrine, and melanoma primaries, while hypovascular deposits most commonly arise from lung, gastric, breast, and colorectal carcinoma [14, 22]. Metastatic lesions with central necrosis may have a partly cystic appearance. Mucin-secreting metastases from the GI tract may demonstrate calcifications [13]. On US, metastases appear non-specific. They may be homogeneous, have a target-sign appearance, show cystic and/or calcified components, and be of increased or decreased reflectivity [9].

On CT, most metastatic lesions are hypoattenuating on unenhanced images and remain so on portal phase images. Hypervascular tumors are often visible as low-attenuation lesions on unenhanced images, enhance avidly in the arterial phase, then fade to isointensity or wash out to hypodensity in the portal or delayed phases. CT is the most sensitive method for detecting the subtle calcifications that may occur within mucin-secreting metastases of GI tract origin.

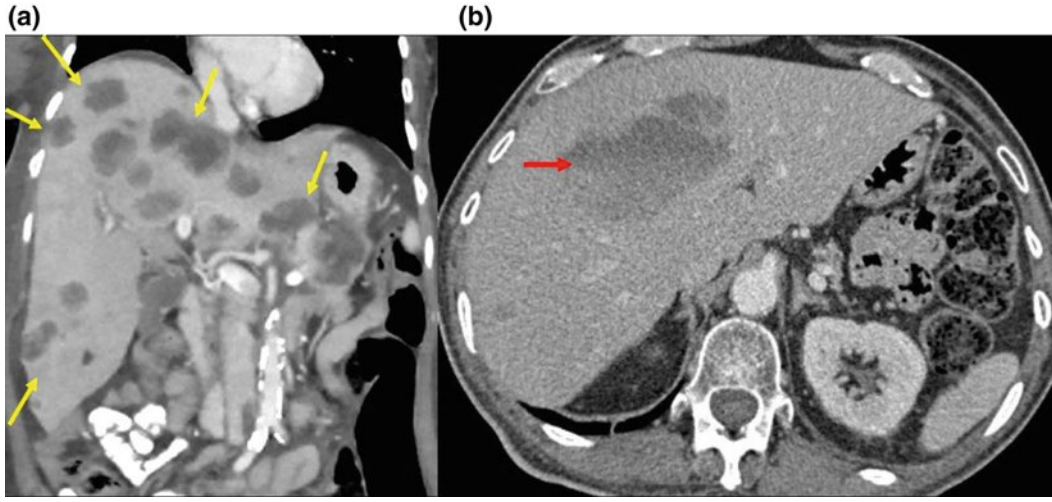

Fig. 2.10 Coronal image from an enhanced CT scan showing multiple, scattered hypodense metastatic liver lesions from colon cancer (*yellow arrows*) (**a**). Axial image from an enhanced CT scan showing a hemorrhagic metastatic lesion with dense blood layering in the lesion (*red arrow*) (**b**)

Central necrosis and rim enhancement can also be clearly demonstrated on CT [13].

On MRI, the majority of metastases are of low signal on T1W and high signal on T2W images. However, lesions with hemorrage or melanoma may have a high signal on T1-weighted imaging. Lesions with a hyperintense viable rim on T2-weighted imaging and hypointense necrotic center have a characteristic "target-sign" appearance [14]. Contrast-enhanced MR studies give similar appearances to CT for the detection and demonstration of lesions in the unenhanced, arterial, and portal phases. Hepatobiliary-specific contrast serves to increase the signal difference between metastatic lesions and background parenchyma thereby increasing their detection [14, 44]. On colloid radionuclide imaging, the majority of metastases appear as areas of reduced activity due to a lack of Kupffer cells.

Studies comparing the relative sensitivity and specificity of cross-sectional imaging techniques in the detection of hepatic metastases can be difficult to evaluate because of variations of technique, methods of validation, and the rapid evolution of imaging technology. For example, in one systematic review, the sensitivities of MRI (after 2004), CT, and PET/CT in detecting colorectal cancer (CRC) liver metastasis in patients without prior chemotherapy treatment were 85, 74, and 66%, respectively [45]. The sensitivities dropped for MRI and CT to 60 and 47%, respectively, for lesions less than one cm.

Post neoadjuvant chemotherapy, the sensitivities were 86, 70, and 52% for MRI, CT, and PET/CT, respectively [46]. In clinical practice, the choice of imaging technique is usually influenced by the likely management implications and local availability and expertise [13].

2.5 Imaging of Irradiated Liver and Liver Tumors

2.5.1 Imaging of Irradiated Normal Liver

Radiographic characterization of irradiated liver tumors and normal liver parenchyma is challenging and can require close collaboration between the diagnostic radiologist and treating radiation oncologist. Herfarth and colleagues described three types of focal radiographic appearances (on CT scan with multiphase contrast) in patients with liver tumors irradiated with high single-fraction radiation doses [47]. In the type I reaction, the liver parenchyma irradiated past a threshold dose appeared hypodense in portal venous phase imaging, and isodense in late-phase imaging; in the type II reaction, the liver parenchyma was hypodense in portal venous phase imaging and hyperdense in late-phase imaging; in the type III reaction, the liver parenchyma was isodense or hyperdense in portal venous phage imaging and hyperdense in late-phase imaging. The reactions appeared to follow a temporal pattern, with the type III reaction following type I and II reactions in sequence. The authors postulated that the type II reaction appearance is related to the veno-occlusive histopathologic findings seen in irradiated liver tissue. Obstruction of venous inflow of contrast to damaged liver tissue would make it hypodense relative to undamaged liver tissue that is well perfused during the portal venous phase of imaging. In late-phase imaging, contrast would now be presented in the damaged liver tissue and it would appear hyperdense relative to the rest of the liver parenchyma. Olsen and colleagues provided support for this model in a study with both radiographic and histopathologic imaging of high-dose irradiated liver [48]. Figure 2.11 shows early (3 months) post-imaging changes consistent with a type II reaction in a patient with hepatocellular carcinoma treated with stereotactic radiation therapy.

2.5.2 Imaging of Irradiated Liver Tumors

Arterial phase contrast enhancement is a hallmark of hypervascular liver tumors such as hepatocellular carcinoma. Embolization and radiofrequency ablation can directly affect blood vessels through occlusion and/or direct ablation. Thus, eradicated tumors that have been treated with these

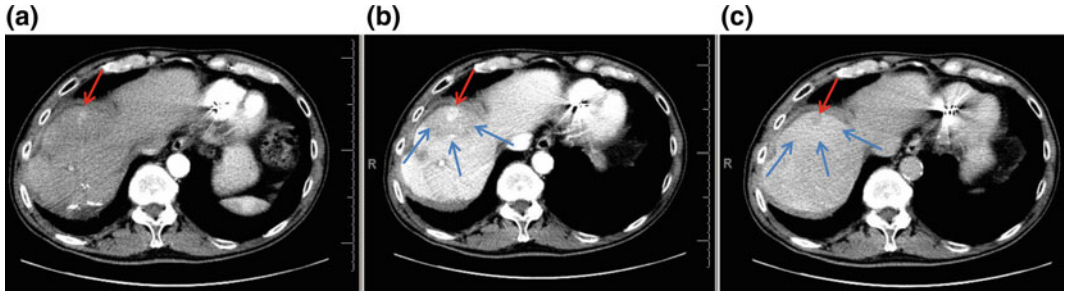

Fig. 2.11 Axial images of a segment eight hepatocellular carcinoma lesion treated with stereotactic radiation therapy. **a** Arterial phase imaging showing contrast enhancement (*red arrow*), **b** portal venous phase imaging showing continuing enhancement (*red arrow*) with a surrounding rim of injured, hypodense liver (*blue arrows*), **c** delayed-phase imaging with washout of contrast from the tumor and subtle hyperenhancement of the immediately surrounding liver (*blue arrows*)

approaches will lose contrast enhancement, and this is considered to be associated with induction of tumor necrosis. The European Association for the Study of the Liver (EASL) guidelines call for post-treatment measurement of the enhancing area of treated tumors, distinct from traditional RECIST criteria, which measures overall tumor size. The AASLD adopted the assessment of tumor necrosis (loss of contrast enhancement), as opposed to assessment of tumor size, in what is known as modified RECIST (mRECIST) criteria, and recommended that this be used in future studies of novel therapies for the treatment of hepatocellular cancer [49]. As discussed elsewhere in this book, radiation therapy differs from embolization and thermal ablations with respect to the manner and kinetics of tumor cell kill, as well as effects on blood vessels. Thus, changes in enhancement patterns, and overall tumor size, may differ post-radiation as compared with interventional approaches. Price et al. reported on the time course of contrast and tumor size changes following high-dose stereotactic radiation therapy for hepatocellular carcinoma. There was a gradual and progressive loss of contrast enhancement which paralleled a decrease in tumor size (with tumor size reduction less pronounced), continuing to 12 months following the completion of radiation [50].

PET and various sequences on MRI may also be helpful in determining the response of treated liver tumors to radiation as well. A sustained decrease in the maximum SUV value following treatment indicates tumor response, whereas an increase in FDG avidity is suspicious for residual cancer [51]. On MR imaging, changes in diffusion-weighted signal intensity as well as T2 signal hyperintensity can be followed to assess lesion response [51].

References

1. Kekis P, Kekis B. Surgical anatomy of the liver. In: Liver and Biliary Tract Surg. Vienna: Springer; 2006. pp. 17–33.
2. Webb WR, Brant WE, Major NM. Fundamentals of body CT. Elsevier Health Sciences. 5 Sep 2014. pp. 188–213.
3. Sibulesky L. Normal liver anatomy. Clin Liver Dis. 2013 Mar 1;2(S1).
4. Lim MC, Tan CH, Cai J, Zheng J, Kow AW. CT volumetry of the liver: where does it stand in clinical practice? Clin Radiol. 2014;69(9):887–95.
5. L'Herminé C. Normal hepatic circulation—anatomy and physiology. In: Radiol of Liver Circ. Netherlands: Springer;1985. pp. 1–3.
6. Lafortune M, Madore F, Patriquin H, Breton G. Segmental anatomy of the liver: a sonographic approach to the Couinaud nomenclature. Radiology. 1991;181(2):443–8.
7. O'Neil M, Damjanov I, Taylor RM. Normal liver. In: Liver Pathology for Clinicians. Springer International Publishing;2015. pp. 1–9.
8. Gelfand DW. The liver: plain film diagnosis. Semin Roentgenol. 1975;10(3):177–85. WB Saunders.
9. Nisenbaum HL, Rowling SE. Ultrasound of focal hepatic lesions. Semin Roentgenol. 1995;30(4): 324–46. WB Saunders.

10. McNaughton DA, Abu-Yousef MM. Doppler US of the liver made simple 1. Radiographics. 2011;31 (1):161–88.
11. Sandstede JJ, Tschammler A, Beer M, Vogelsang C, Wittenberg G, Hahn D. Optimization of automatic bolus tracking for timing of the arterial phase of helical liver CT. Eur Radiol. 2001;11(8):1396–400.
12. Sahani DV, Singh AH. Dual-phase liver MDCT. In: MDCT: a pract approach. Milan: Springer; 2006. pp. 39–48.
13. Sica GT, Ji H, Ros PR. CT and MR imaging of hepatic metastases. Am J Roentgenol. 2000;174 (3):691–8.
14. Namasivayam S, Martin DR, Saini S. Imaging of liver metastases: MRI. Cancer Imaging. 2007;7(1):2.
15. Liu PS, Hussain HK. Contemporary and emerging technologies in abdominal magnetic resonance imaging. Semin Roentgenol. 2013;48(3):203–13. Elsevier.
16. Katabathina VS, Dasyam AK, Dasyam N, Hosseinzadeh K. Adult bile duct strictures: role of MR imaging and MR cholangiopancreatography in characterization. Radiographics. 2014;34(3):565–86.
17. Seale MK, Catalano OA, Saini S, Hahn PF, Sahani DV. Hepatobiliary-specific MR contrast agents: role in imaging the liver and biliary tree 1. Radiographics. 2009;29(6):1725–48.
18. Kinnard MF, Alavi A, Rubin RA, Lichtenstein GR. Nuclear imaging of solid hepatic masses. Semin Roentgenol. 1995;30(4)375–95. WB: Saunders.
19. Kim JY, Kim MH, Lee TY, Hwang CY, Kim JS, Yun SC, Lee SS, Seo DW, Lee SK. Clinical role of 18F-FDG PET-CT in suspected and potentially operable cholangiocarcinoma: a prospective study compared with conventional imaging. Am L Gastroenterol. 2008;103(5):1145–51.
20. Schlant RC, Galambos JT, Shuford WH, Rawls WJ, Winter TS, Edwards FK. The clinical usefulness of wedge hepatic venography. Am J Med. 1963;35 (3):343–9.
21. Halefoglu AM. Magnetic resonance cholangiopancreatography. Semin Roentgenol. 2008;43(4):282–9. WB: Saunders.
22. Maniam S, Szklaruk J. WJR. World. 2010;2(8): 309–22.
23. Wachsberg RH, Bahramipour P, Sofocleous CT, Barone A. Hepatofugal flow in the portal venous system: pathophysiology, imaging findings, and diagnostic pitfalls 1. Radiographics. 2002;22 (1):123–40.
24. Gupta AA, Kim DC, Krinsky GA, Lee VS. CT and MRI of cirrhosis and its mimics. Am J Roentgenol. 2004;183(6):1595–601.
25. Sangster GP, Previgliano CH, Nader M, Chwoschtschinsky E, Heldmann MG. MDCT imaging findings of liver cirrhosis: spectrum of hepatic and extrahepatic abdominal complications. HPB Surg. 2013;6:2013.
26. Tappouni R, Sakala MD, Hosseinzadeh K. Mimics of Hepatic Neoplasms. Semin Roentgenol. 2015;50 (4):305–19. Elsevier.
27. Watanabe A, Ramalho M, AlObaidy M, Kim HJ, Velloni FG, Semelka RC. Magnetic resonance imaging of the cirrhotic liver: an update. World J Hepatol. 2015;7(3):468.
28. Yilmaz S, Yekeler E, Rozanes I. Hepatobiliary and pancreatic: Gamna–Gandy bodies of the spleen. J Gastroen Hepatol. 2007;22(5):758.
29. Aspestrand F, Kolmannskog F. CT and angiography in chronic liver disease. Acta Radiol. 1992;33 (3):251–4.
30. Clark HP, Carson WF, Kavanagh PV, Ho CP, Shen P, Zagoria RJ. Staging and current treatment of hepatocellular carcinoma 1. Radiographics. 2005;25(suppl_1):S3–23.
31. Hanna RF, Aguirre DA, Kased N, Emery SC, Peterson MR, Sirlin CB. Cirrhosis-associated hepatocellular nodules: correlation of histopathologic and MR imaging features 1. Radiographics. 2008;28 (3):747–69.
32. ACR (American College of Radiology). Liver imaging reporting and data system. http://www.acr.org/Quality-Safety/Resources/LIRADS.
33. Tublin ME, Dodd GD 3rd, Baron RL. Benign and malignant portal vein thrombosis: differentiation by CT characteristics. Am J Roemtgenol. 1997;168 (3):719–23.
34. Hussain SM, Reinhold C, Mitchell DG. Cirrhosis and lesion characterization at MR imaging 1. Radiographics. 2009;29(6):1637–52.
35. Yamashita Y, Takahashi M, Baba Y, Kanazawa S, Charnsangavej C, Yang D, Wallace S. Hepatocellular carcinoma with or without cirrhosis: a comparison of CT and angiographic presentations in the United States and Japan. Abdom Imaging. 1993;18(2):168–75.
36. McEvoy SH, McCarthy CJ, Lavelle LP, Moran DE, Cantwell CP, Skehan SJ, Gibney RG, Malone DE. Hepatocellular carcinoma: illustrated guide to systematic radiologic diagnosis and staging according to guidelines of the American Association for the Study of Liver Diseases. Radiographics. 2013;33(6):1653–68.
37. Purysko AS, Remer EM, Coppa CP. Leão Filho HM, Thupili CR, Veniero JC. LI-RADS: a case-based review of the new categorization of liver findings in patients with end-stage liver disease. Radiographics. 2012;32(7):1977–95.
38. Mitchell DG, Bruix J, Sherman M, Sirlin CB. LI-RADS (liver imaging reporting and data system): summary, discussion, and consensus of the LI-RADS management working group and future directions. Hepatology. 2015;61(3):1056–65.
39. Blechacz BR, Gores GJ. Cholangiocarcinoma. Clin Liver Dis. 2008;12(1):131–50.
40. Engelbrecht MR, Katz SS, van Gulik TM, Laméris JS, van Delden OM. Imaging of perihilar cholangiocarcinoma. Am J Roentgenol. 2015;204(4):782–91.

41. Chung YE, Kim MJ, Park YN, Choi JY, Pyo JY, Kim YC, Cho HJ, Kim KA, Choi SY. Varying appearances of cholangiocarcinoma: radiologic-pathologic correlation 1. Radiographics. 2009;29 (3):683–700.
42. Sainani NI, Catalano OA, Holalkere NS, Zhu AX, Hahn PF, Sahani DV. Cholangiocarcinoma: current and novel imaging techniques 1. Radiographics. 2008;28(5):1263–87.
43. Soulen MC. Angiographic evaluation of focal liver masses. In Semin Roentgenol. 1995;30(4):362–74.
44. Oliva MR, Saini S. Liver cancer imaging: role of CT, MRI, US and PET. Cancer Imaging. 2004.4 Spec No A:S42.
45. Niekel MC, Bipat S, Stoker J. Diagnostic imaging of colorectal liver metastases with CT, MR imaging, FDG PET, and/or FDG PET/CT: a meta-analysis of prospective studies including patients who have not previously undergone treatment 1. Radiology. 2010;257(3):674–84.
46. van Kessel CS, Buckens CF, van den Bosch MA, van Leeuwen MS, van Hillegersberg R, Verkooijen HM. Preoperative imaging of colorectal liver metastases after neoadjuvant chemotherapy: a meta-analysis. Ann Surg Oncol. 2012;19(9):2805–13.
47. Herfarth KK, Hof H, Bahner ML, et al. Assessment of focal liver reaction by multiphasic CT after stereotactic single-dose radiotherapy of liver tumors. Int J Radiat Oncol Biol Phys. 2003;57:444–51.
48. Olsen CC, Welsh J, Kavanagh BD, et al. Microscopic and macroscopic tumor and parenchymal effects of liver stereotactic body radiotherapy. Int J Radiat Oncol Biol Phys. 2009;73:1414–24.
49. Lencioni R, Llovet JM. Modified RECIST (mRECIST) assessment for hepatocellular carcinoma. Semin Liver Dis. 2010;30(1):52–60.
50. Price TR, Perkins SM, Sandrasegaran K, et al. Evaluation of response after stereotactic body radiotherapy for hepatocellular carcinoma. Cancer. 2012;118:3191–8.
51. Haddad MM, Merrell KW, Hallemeier CL, et al. Stereotactic body radiation therapy of liver tumors: post-treatment appearances and evaluation of treatment response: a pictorial review. Abdom Radiol (NY). 2016;41:2061–77.

http://www.springer.com/978-3-319-54530-1

Radiation Therapy for Liver Tumors
Fundamentals and Clinical Practice
Meyer, J.; Schefter, T. (Eds.)
2017, XVIII, 288 p. 62 illus., 46 illus. in color., Softcover
ISBN: 978-3-319-54530-1